

1       **Rapid duplexed detection of illicit drugs in wastewater using gold**  
2                               **nanoparticle conjugated aptamer sensors**

3                               Kang Mao<sup>a</sup>, Jun Ma<sup>b</sup>, Xiqing Li<sup>a</sup>, and Zhugen Yang<sup>c\*</sup>

4                               <sup>a</sup> *Laboratory for Earth Surface Processes, College of Urban and Environmental*  
5                               *Sciences, Peking University, Beijing 100871, China*

6                               <sup>b</sup> *Guangzhou Huali Science and Technology Vocational College, Guangzhou, 511325,*  
7                               *China*

8                               <sup>c</sup> *School of Water, Environment and Energy, Cranfield University, Cranfield, MK43*  
9                               *0AL, United Kingdom*

10                              Corresponding Email: zhugen.yang@cranfield.ac.uk (Dr Z. Yang)

11       **Abstract:** The abuse of illicit drug addiction is a worldwide public health and social  
12       problem. In this paper, we reported on a simple and rapid colorimetric biosensor for  
13       duplexed detection of methamphetamine (METH) and cocaine in a single assay. Gold  
14       nanoparticles (AuNPs) and Au@Ag NPs were synthesized and functionalized with  
15       DNA reporter probes (RPs) for METH and cocaine, respectively. The magnetic beads  
16       (MBs) were conjugated with two capture probes (CPs) respective to METH and  
17       cocaine. The respective RPs and CPs were designed to hybridize with each illicit  
18       drug-binding DNA aptamers through DNA-DNA hybridization, forming a sandwich  
19       structure. This MBs-based sandwich structure could be removed with an external  
20       magnetic field. However, due to the higher affinity of DNA aptamers with illicit  
21       drugs, the sandwich structure was disassembled when illicit drugs are introduced into  
22       the solution, leading to the colour changes of the supernatant. Utilizing a non-negative  
23       matrix factorization (NMF) algorithm to process the data, we demonstrated the ability

24 of our biosensor for the simultaneous quantification of two illicit drugs. Under the  
25 optimal condition, our sensors were able to detect both METH and cocaine at the nM  
26 level with a wide dynamic range. This sensing platform provides a huge potential on  
27 drug consumption evaluation at the community level for wastewater-based  
28 epidemiology.

29 **Keywords:** illicit drug of abuse, wastewater-based epidemiology, colorimetric  
30 biosensor

### 31 1. **Introduction**

32 Illicit drug abuse has become a global concern considering its close relationship  
33 with the increasing incidence of crimes and severe social problems (Cyranski, 2018;  
34 Galanie et al., 2015; Merz, 2018). Methamphetamine (METH) and cocaine (COC)  
35 and are two of the most widely abused illegal drugs in the world (EMCDDA, 2016;  
36 Merz, 2018; Mokhtarzadeh et al., 2015; Xu et al., 2017). To evaluate the pattern of  
37 illicit drug consumption, a new approach namely wastewater-based epidemiology  
38 (WBE) has emerged in the past decade. Usually, the drug residues and their  
39 metabolites would be excreted by humans in a given area (e.g., a city and a  
40 community) pool in wastewater at a certain wastewater treatment plants. WBE is  
41 conducted by collecting wastewater samples and analysing the concentration of  
42 targets in wastewater, and thereby can be used to monitor the community-wide drug  
43 consumption taking into account population served, stability of drug residues,  
44 excretion rates, and wastewater volumes (Cyranski, 2018; Du et al., 2017; Du et al.,  
45 2018; van Nuijs et al., 2011; Zuccato et al., 2005). Compared to the conventional  
46 population survey method, WBE holds several advantages such as more objective and  
47 much less time-consuming (Du et al., 2018; Ettore et al., 2008), and thus this strategy

48 has been widely used for the monitoring of illicit drugs in many countries (Du et al.,  
49 2017; EMCDDA, 2016; Thomas et al., 2012), including America (Foppe et al., 2018),  
50 Australia (Bade et al., 2019) and many European countries (Castrignanò et al., 2018;  
51 EMCDDA, 2016). To get the concentration of wastewater, the widely employed  
52 analytical instrument is mass spectrometry (MS) coupled with high-performance  
53 liquid chromatography (HPLC), which is robust, highly sensitive and selective (Du et  
54 al., 2015; Gao et al., 2017). But these methods usually need a sample preparation  
55 before illicit drug analysis, such as the purification of raw wastewater with solid phase  
56 extraction. In addition, the compulsory sample preparation usually requires the well-  
57 trained personnel to operate an instrument for analysis and then interpret the data in  
58 the central laboratory. In order to evaluate illicit drugs of abuse, preferably at the site  
59 of sample collection, there is an urgent need to develop rapid, simple and inexpensive  
60 tools for detection illicit drugs in complex environmental samples.

61 As an rapid and cost-effective analytical tool, aptamer biosensor (aptasensor) has  
62 attracted increasing attention for determination of illicit drugs, such as cocaine,  
63 methamphetamine, codeine and ketamine (Asghary et al., 2018; Lodha et al., 2014;  
64 Mao et al., 2018; Mokhtarzadeh et al., 2015; Roncancio et al., 2014). The signal of  
65 sensors from the binding between DNA aptamers and illicit drugs can be detected  
66 with colorimetry (Li et al., 2013), fluorescence (Stojanovic et al., 2000) and Surface-  
67 Enhanced Raman Spectrometry (SERS) (Mao et al., 2018), electrochemistry (Yang et  
68 al., 2016), and other techniques (Neves et al., 2015; Ya et al., 2015). We have recently  
69 developed electrochemical aptamer sensors for the determination of cocaine in  
70 wastewater, which demonstrated the cocaine consumption trends with a weekend  
71 peak based on the sampling in a wastewater treatment plant in the Southwest of  
72 England (Yang et al., 2016). For METH determination, we have developed a new

73 colorimetric strategy using G-quadruplex DNAzyme for the determination of METH  
74 (Mao et al., 2016). Although these assays mentioned above show the great capability  
75 for single illicit drug determination, there are no reports on biosensors for  
76 simultaneous determination of multiple illicit drugs so far. In fact, a variety of illicit  
77 drugs (such as METH, cocaine, et al.) are usually present in the sample at the same  
78 time, which are widely distributed and transported in natural water and wastewater  
79 (EMCDDA, 2016). Although one can use several biosensors for the determination of  
80 various targets separately, it is costly and time-consuming. Thus, there is a great need  
81 for the development of simultaneous determination of multiplexed illicit drugs within  
82 a single assay. This may provide opportunities for the monitoring of illicit drugs at a  
83 trace level in the environment matrixes.

84 The rapid development of nanomaterial-related technologies (Tang et al., 2018)  
85 provides a huge opportunity for designing selective and sensitive aptasensors for the  
86 determination of illicit drugs. For example, recent development and applications of  
87 nanomaterial-based illicit drug aptasensors by using optical and electrochemical  
88 analytical techniques for illicit drugs determination have been reviewed (Kumar et al.,  
89 2018; Mokhtarzadeh et al., 2015). In these nanomaterials, AuNPs has been widely  
90 used to improve the sensitivity due to their unique properties such as facile  
91 preparation methods and excellent optical properties (Shen et al., 2010; Xie et al.,  
92 2011). Magnetic beads, have been widely applied for determination and separation  
93 due to their wonderful magnetic separation characteristics, excellent binding kinetics,  
94 good maneuverability, and biological targeting properties (Song et al., 2014; Wen et  
95 al., 2014). However, to our knowledge, the analytical method based on the  
96 combination of gold nanoparticles and MBs for the multiplexed determination of  
97 illicit drugs has not yet been reported.

98 Hence, we designed a new biosensing strategy for the simultaneous multiplexed  
99 determination of illicit drugs in a single assay, which offers a rapid signal response of  
100 targets through simply mixing DNA aptamers for signal readout. Our platform based  
101 on non-aggregated AuNPs together with magnetic beads displayed high selectivity  
102 and sensitivity towards the targets, which holds unique advantages by comparing  
103 classical colorimetric method and could be extend for more wide application. Because  
104 AuNPs coated with silver-Au@Ag show similar determination capability with AuNPs  
105 but with different optical signals, we combined Au@Ag NPs with AuNPs together to  
106 develop a colorimetric system for multiplexed determination of METH and cocaine.  
107 In order to prevent ambiguities related to colour determination by visual assay, we  
108 introduced a data algorithm analysis system based on functional non-negative matrix  
109 factorization (NMF) for targets quantification, which was consistent with the  
110 colorimetric result. According to this finding, the feasibility of non-aggregated metal  
111 NPs colorimetric determination of two illicit drugs in a single assay was demonstrated  
112 for the first time. We believed that colorimetric analysis based on the combination of a  
113 non-aggregated noble metal nanoparticle and NMF analysis has a huge potential as a  
114 generic platform for the multiplexed determination of a variety of targets.

## 115 **2. Materials and Methods**

### 116 **2.1. Materials**

117 All oligonucleotide sequences were purified by HPLC and ordered from Sangon  
118 Biotech Co. Ltd. (Shanghai, China) (detailed in Table S1). Carboxyl-modified  
119 magnetic beads (MBs, 1.05  $\mu\text{m}$  Dynabeads<sup>TM</sup> My One<sup>TM</sup>, 10 mg mL<sup>-1</sup>) were bought  
120 from Thermo Fisher Scientific. Chloroauric acid (HAuCl<sub>4</sub>·3H<sub>2</sub>O) and silver nitrate  
121 (AgNO<sub>3</sub>) were ordered from Shanghai Chemical Reagent (Shanghai, China) Co., Ltd.  
122 All illicit drugs and metabolites, including METH and cocaine were bought from

123 Cerilliant (Round Rock, USA). The ultrapure water is purified using a Millipore  
124 filtration system (18.2 MΩ·cm) in the whole experiments. All experiments were  
125 performed in compliance with the relevant laws and institutional guidelines, and all  
126 reagents in this experiment have been agreed by the institutional committee (Peking  
127 University, the People's Republic of China).

## 128 **2.2. Instrumentation**

129 A Scanning Electron Microscope (SEM) (ZEISS, SIGMA) was used to obtain the  
130 SEM pictures of AuNPs and Au@Ag. A JEM-2100 (HR, Japan) microscope was  
131 utilized to obtain the TEM images of AuNPs and Au@Ag NPs. UV-vis spectra of  
132 AuNPs and Au@Ag were recorded by Lambda 35 UV-vis spectrometer (Perk Elmer,  
133 USA) through 80 μL quartz cells with a path length of 1 cm.

## 134 **2.3. Synthesis of AuNPs and Au@Ag**

135 In this experiment, AuNPs stabilized by citrate were synthesized as follows: 50 mL  
136 HAuCl<sub>4</sub> (0.01%, w/w) was reduced by addition 750 μL trisodium citrate (1%, w/w) at  
137 120 °C using magnetic stirring for 25 minutes until the obtained reaction mixtures  
138 turned to be wine red. Au@Ag NPs were synthesized in a seed-mediated method  
139 following the previous report (Shen et al., 2010). Firstly, 600 μL 0.5 % (w/w) AgNO<sub>3</sub>  
140 solution was introduced to boiling gold seed solution (100 mL). Then, 1 mL 1 %  
141 (w/w) sodium citrate solution as the reducing agent was introduced dropwise under  
142 stirring. The mixture was boiled for 1 h and Au@Ag was ready to use after cooling  
143 down.

## 144 **2.4. The preparation of RPs and CPs**

145 The RPs were prepared as follows: The two types of NPs were conjugated with the  
146 different RP DNA sequences by treating citrate-stabilized nanoparticles with a  
147 solution containing thiol-modified oligonucleotides, respectively (Figure S1A). 15

148 nmol thiolated RP DNA sequence was introduced to 5 ml Au@Ag NPs or AuNPs  
149 nanoparticles suspended in PB buffer. After 24 h incubation, 2 M NaCl was  
150 introduced to reach the salt concentration at 0.05 M and then increased to 0.1 M after  
151 standing for 8 h. The nanoparticles were isolated through centrifugation and washed  
152 with PBS-T solution after aging in 0.1 M NaCl for two days.

153 The CPs were prepared as follows: The carboxylated MBs were conjugated with  
154 the CP DNA following the manufacturer's protocol. 2.5 mL carboxylated MBs were  
155 washed two times with 2.5 mL MES solution and the MBs were re-suspended in 250  
156  $\mu$ L MES buffer before immobilization. The mixture of 36.2 nmol amino-modified CP  
157 DNA and 36.2  $\mu$ mol EDC HCl was introduced to MBs solution and incubated at 25 °C  
158 by gently shaking overnight. In the end, to quench excess activated carboxylic acid  
159 groups on the surface of MBs, the MBs were incubated with 50 mM Tris solution for  
160 15 minutes at 25 °C by gently shaking. The coated MBs were washed three times  
161 using 2.5 mL Tris solution and then re-suspended in PBS-T solution for use.

## 162 **2.5. Elaboration and optimization of biosensors**

### 163 **2.5.1. Elaboration of biosensors**

164 As shown in Scheme 1, this sensing platform consisted of a CP, RP and an  
165 aptamer. The aptamer bound CP and RP through hybridization forms a double-  
166 stranded DNA (dsDNA). After removing Au@Ag NPs-DNA-MBs or AuNPs-DNA-  
167 MBs complex by an external magnetic field, we can observe a decreased absorbance  
168 signal of Au@Ag solution. However, the target illicit drugs can prevent the formation  
169 of dsDNA due to a higher affinity between the targets and the designed aptamer. The  
170 dose of illicit drugs could generate a different signal that can be measured by a UV-  
171 vis spectrometer.

172 To evaluate the feasibility of the biosensing mechanism, a typical non-aggregated

173 Au@Ag nanosensor for METH determination was acted as a case study. 5  $\mu\text{L}$  METH  
174 (cocaine, 5  $\mu\text{M}$ ) was mixed with 5  $\mu\text{L}$  of 1.2  $\mu\text{M}$  METH aptamer (or 1  $\mu\text{M}$  cocaine  
175 aptamer) solutions, followed through adding 20  $\mu\text{L}$  PBS-T solution. After incubation  
176 for 30 minutes, 1  $\mu\text{L}$  CP and 50  $\mu\text{L}$  RP were introduced to the mixture and then  
177 hybridized reaction with gentle shaking for 90 minutes. The total volume was kept at  
178 150  $\mu\text{L}$  by added PBS-T solution. After hybridization reaction, the magnetic beads  
179 with target-linked AuNPs or Au@Ag NPs together with unreacted MBs were  
180 removed by using an external magnetic field. We can measure the supernatant for  
181 signal readout after the separation by a UV-vis spectrometer in 80  $\mu\text{L}$  quartz micro-  
182 cuvette at 25  $^{\circ}\text{C}$ .

183 We also carried out control experiments with following mixtures: CP and RP; CP,  
184 RP, and illicit drug; CP, RP, and aptamer. In our experiment, each component was  
185 introduced as the same volume and concentration as in the presence of METH or  
186 cocaine. A certain volume of PBS-T solution was added into the mixture to obtain a  
187 150  $\mu\text{L}$  constant volume in total.

### 188 **2.5.2. Optimization of the determination conditions**

189 The MBs concentration had a significant effect on the sensitivity of the assay  
190 because the ratio between the CPs and RPs would change. To ensure a highly  
191 sensitive analysis, a series of MBs concentration from 3.3  $\mu\text{g L}^{-1}$  to  $3.3 \times 10^2 \mu\text{g L}^{-1}$   
192 (3.3, 6.6,  $3.3 \times 10^1$ ,  $6.6 \times 10^1$  and  $3.3 \times 10^2 \mu\text{g L}^{-1}$ ) were tested under the same  
193 conditions to get the optimal concentration of the MBs.

194 The hybridization time was also a significant parameter for colorimetric assay. The  
195 hybridization time was studied through measuring the peak intensities of UV-vis  
196 spectra. The time interval was recorded 15 minutes a time ranging 0-105 minutes.

197 The optimal METH aptamer concentration which may influence the UV-vis spectra



198 of Au@Ag NPs and AuNPs was determined by recording peak intensities of UV-vis  
199 spectra at 400 nm and 520 nm, respectively. The biosensor was optimized with the  
200 various aptamer concentrations (METH aptamer: 0, 10, 20, 30, 40, 50, and 60 nM;  
201 COC aptamer: 0, 10, 20, 30, 40, and 50 nM).

## 202 **2.6. Analytical performance evaluation**

203 Under the optimal conditions, we evaluated the sensitivity of the sensor to detect  
204 METH by testing various METH concentrations ranging from 0 nM to 200 nM and  
205 cocaine from 0 to 150 nM.

206 The selectivity of the sensor was examined by comparing the result with seven  
207 common illicit drugs and metabolites, namely cathinone (CAT), methcathinone  
208 (MCAT), 3-trifluoromethylphenylpiperazine (BZP), ketamine (KET), morphine  
209 (MOR), norketamine (NK), and MDA. The experiment followed the same procedure  
210 for the determination of other drugs and metabolites at 1  $\mu$ M, the response of which  
211 was compared with the signal from METH and cocaine at 50 nM.

212 To explore the performance of our developed biosensors in real applications,  
213 effluent wastewater samples (collected from Xiaojiahe Wastewater Plant in Beijing,  
214 China) were filtered with 0.22  $\mu$ m microporous membrane to remove suspended  
215 particulate matter (SPM), followed by spiking METH and cocaine into the wastewater  
216 for a final concentration at 75 nM. Spiked wastewater was detected by our biosensor.

## 217 **2.7. Non-negative matrix factorization (NMF) analysis**

218 “Multiplicative” iteration rules-based NMF was a multi-variant analytical system  
219 by non-negative constraints for the generation of the approximate data and application  
220 in an analytical science (Berry et al., 2007; Xie et al., 2011). The principle of NMF  
221 analysis that processed the UV-vis spectra in this experiment as shown in Figure 1:  
222 Given one initial non-negative matrix ( $V$ ), it could find two different non-negative

223 matrices to approximate the original matrix. The one was the basis matrix ( $W$ ) and the  
224 other one was the coefficient matrix ( $H$ ). When conducting data analysis, all UV-vis  
225 spectra were combined to form matrix  $V$ . The number of factors would be set as 2 due  
226 to that two nanoparticles (Au@Ag and AuNPs) existed in the solution. Low-rank  
227 matrices  $H$  and  $W$  automatically started from random matrices and stopped while the  
228 matrix doesn't change for 10,000 iterations. Matrix  $H$  corresponded to the intensity  
229 coefficient and  $W$  corresponded with the basic spectra for pure Au@Ag NPs and  
230 AuNPs. UV-vis spectra results were exported from the instrument software and  
231 imported into MATLAB where NMF data processing was performed to directly  
232 quantify of METH and COC.

### 233 **3. Results and discussion**

#### 234 **3.1. Colorimetric sensing principal for METH and cocaine**

235 The AuNPs and Au@Ag NPs were synthesized and characterized by UV-vis  
236 spectrometer, SEM and HR-TEM. As shown in Figure 2, AuNPs and Au@Ag NPs  
237 were approximately 40 nm with a uniform size (Figure 2b and Figure 2c). Figure 2 (d)  
238 indicated a thinner silver layer surrounds the gold core because of the different  
239 contrast between these two materials. Figure 2a demonstrated that the UV-vis spectra  
240 of Au@Ag NPs and AuNPs. The UV-vis signal peaks of Au@Ag and AuNPs were  
241 400 nm and 520 nm, respectively. Compared with the absorption peak of AuNPs, the  
242 peak of Au@Ag NPs solution was blue-shifted because Au@Ag NPs and AuNPs  
243 with the same particle size had different surface plasmon resonance (SPR)  
244 frequencies. This will facilitate to reduce the interference caused by the overlapping  
245 peaks when simultaneously detecting cocaine and METH.

246 The working principle of our colorimetric biosensor was shown in Scheme 1. We  
247 tried to design two MBs-modified capture probe (CPs), one AuNPs and the other

248 Au@Ag NPs labelled reporter probe (RPs), and two aptamers which specifically  
249 bound with METH and COC, respectively. The CPs were superparamagnetic MBs  
250 with a carboxyl coating, and it would facilitate sample separation when activated by  
251 an external magnetic field. These MBs were functionalized with aminated  
252 oligonucleotides (CP DNA) with EDC·HCl as the linker, which could match fully one  
253 part of target sequence but different from the fragment complementary with RP DNA  
254 (see Figure S1B). The RPs were either Au@Ag NPs or AuNPs modified with RP  
255 DNA sequence which is partially complementary to the aptamer. Herein, each  
256 aptamer was complementary with its respective MB-conjugated CP DNA and  
257 nanoparticle-conjugated RP DNA, then forming a NPs-dsDNA-MBs sandwich  
258 structure, for both METH and cocaine.

259 To establish the multiplexed sensors for METH and COC determination, the  
260 mixtures in solution containing METH RP, METH CP, COC RP, and COC CP, and  
261 two DNA aptamers for illicit drugs were introduced into the solution. After the  
262 hybridization, an external magnetic field was able to adsorb the MBs-conjugated  
263 complexes, leading to the bound metal nanoparticle decreasing and color changes in  
264 the supernatant. However, in the presence of the target drugs, NPs-dsDNA-MBs  
265 sandwich structure complex can't be generated because of higher affinity between the  
266 aptamer and the target than that from DNA-DNA hybridization. Furthermore, the  
267 color of the supernatant depended on the amount of two illicit drugs added to the  
268 solution. This interesting color change was useful for simultaneous determination of  
269 two targets from a single assay, enabling a novel colorimetric approach for the  
270 determination of two illicit drugs. Furthermore, this determination strategy avoided  
271 the aggregation between optical noble nanoparticles and the sedimentation, which  
272 would be beneficial to minimize the non-specific interference response. Due to that

273 this method only affected the peak intensity rather than the peak position, the UV-vis  
274 spectra signal featured an inherent simplicity for quantification.

### 275 3.2. Detection conditions optimization

276 We optimized a range of detection parameters to improve the sensitivity of our  
277 sensors, including the concentration of MBs, the binding time to generate NPs-  
278 dsDNA-MBs structure and the aptamer concentration. The optimized concentration of  
279 the MBs was determined to be  $66.7 \mu\text{g L}^{-1}$ , showing in Figure S2. The results also  
280 suggested that the concentration of magnetic beads used to remove AuNPs is the same  
281 as that of Au@Ag.

282 The reaction time for the formation of NPs-dsDNA-MB was an important  
283 parameter for the evaluation of our sensors. Aptamers were introduced and the time  
284 set as 0 minutes, and the spectra signal changes are observed. The maximum  
285 absorption value of METH and cocaine (Figure S3) were recorded after the addition  
286 of DNA aptamers against METH and cocaine, respectively. The incubation was  
287 maintained at 25 °C for 110 minutes. Figure S3 demonstrated that the intensity of the  
288 UV-vis signal gradually decreased after the addition of the aptamer, and had a  
289 minimum value at 60 minutes. Therefore, we used the optimized 60 minutes for our  
290 assay.

291 The optimal concentration of DNA aptamers to quench the UV-vis signal of  
292 Au@Ag NPs and AuNPs were detected by obtaining absorbance intensities at 400 nm  
293 and 520 nm, respectively. Analysis of the plots in Figure S3c showed that the UV-vis  
294 signal of AuNPs decreased with increasing METH aptamer concentrations and nearly  
295 complete quenching occurred over 60 nM. In this process, it should be noted that if  
296 there is excessive METH aptamers, it may result in non-specific (i.e., no surface  
297 plasmon resonance enhancement) binding of the aptamer to the METH. As a result,

298 40 nM METH aptamer was optimized in this biosensor. Importantly, we observed  
299 METH obviously blocking of the quenching of the AuNPs by 40 nM aptamer,  
300 returning the UV-vis intensity of Au@Ag NPs up to 89.1% compared with its initial  
301 value (Figure S3c). Similarly, 30 nM cocaine aptamer was optimized and chosen for a  
302 sensitive assay (Figure S3d).

### 303 3.3. Determination of single illicit drug with our sensors

304 To check the feasibility of the sensing platform, the single-target model was firstly  
305 to test in our experiment. Firstly, the effects of this analytical method without or with  
306 METH, on the UV-vis signal of AuNPs nanoparticles were determined. As shown in  
307 the result, in a control experiment, stronger absolute absorbance intensity was  
308 observed (Figure 3a, MBs + AuNPs). When METH is introduced, the signal intensity  
309 of absorbance had no significant change (Figure 3a, MBs + AuNPs + METH), which  
310 indicated that only METH alone had almost no interference to this assay. However,  
311 once the addition of METH aptamer in the solution, the signal intensity of absorbance  
312 decreased dramatically (Figure 3a, MBs +AuNPs + Apt), due to the formation of the  
313 AuNPs-dsDNA-MBs sandwich structure according to the base pair matching  
314 principle. The complex would subsequently be eliminated by an external magnetic  
315 field. The removal of AuNPs nanoparticles decreased the absorbance intensity. When  
316 both METH and its corresponding aptamer were present, the absorbance drastically  
317 recovered (Figure 3a, MBs + AuNPs + Apt + METH). The signal was a little lower  
318 than the absolute absorbance intensity of AuNPs nanoparticles. The increase in signal  
319 intensity of UV-vis spectra with both METH and METH aptamer was due to the  
320 formation of METH-aptamer complex, which prevented the formation of the  
321 sandwich structure complex and therefore prevented the external magnetic field from  
322 removing the AuNPs nanoparticles. Similarly, in the absence of cocaine, Au@Ag NPs

323 can hybridize with aptamer to form a sandwich structure through DNA-DNA  
324 hybridization (Figure 3b, MBs + Au@Ag + Apt). When using an external magnetic  
325 field, the original deep yellow colour of the supernatant became light yellow.  
326 However, when introducing cocaine into the solution, the absorbance was drastically  
327 recovered and confirmed that it's the presence (Figure 3c, MBs + Au@Ag + Apt +  
328 COC). Hence, the color change of supernatant by certain illicit drugs demonstrated  
329 that it was feasible to use the platform for the duplexed determination of illicit drugs.

330 The intensity of peaks at 520 nm assigned to UV-vis signal from AuNPs clearly  
331 increased with the addition of the METH. Figure 3c showed the linear fit of the signal  
332 intensity of the supernatant solution as the function of the concentration of METH.  
333 The linear range for the detection of METH spanned from 1.0 to 200 nM under  
334 optimized condition. In similar way, when the concentration of cocaine increased, the  
335 signal intensity of the peak at 400 nm associated with Au@Ag NPs increase  
336 noticeably (Figure 3d), which led to the colour change of the supernatant solution  
337 from light yellow to deep yellow different from other reported colorimetric illicit drug  
338 detection method (Shi et al., 2015). The UV-vis spectra signal demonstrated a good  
339 linear change ranging from 10 nM to 150 nM.

#### 340 **3.4. Duplexed detection of illicit drugs in a single assay using NMF analysis**

341 Simultaneous determination of different illicit drugs (METH and cocaine) in a  
342 single assay was performed through our biosensors. There were two directions of  
343 colour conversion (from orange to yellow or red) in this method, our biosensor thus  
344 enabled to run a single assay for the determination of two targets. We evaluated the  
345 feasibility of our biosensors for the determination of both METH and cocaine in a  
346 single assay and the analytical performance from colour changes. A 5×5 matrix was  
347 designed in a microplate, in which each element is a sample containing the different

348 concentrations of METH and cocaine. Figure 4b presented the 5×5 matrix photo  
349 showing the colour change of two illicit drugs at different concentrations in each  
350 microplate. Obviously, the colour change had a significant difference, and varied from  
351 5-200 nM for METH and 1-150 nM for cocaine. Also, the performance of the double-  
352 colour analytical system was evaluated by UV-vis spectra measurements by  
353 constructing a 10×10 matrix varied from 0-200 nM for METH and 0-150 nM for  
354 cocaine, respectively. As shown in Figure 4a, both the absorption peaks of UV-vis  
355 simultaneously increased when the sample containing both METH and cocaine was  
356 introduced. However, the UV-vis spectra of solutions cannot be analyzed as easily as  
357 the visual signals due to the interference and overlap between UV-vis spectra of  
358 Au@Ag NPs and AuNPs. One of the reasons for such interference is that the UV-vis  
359 signal-active nanoparticles are not narrow enough to remove the spectra overlap,  
360 which may make it difficult to quantify it. To clearly analyze the UV-vis spectra signal  
361 and quantify the METH and cocaine, we made full use of NMF to factorize a series of  
362 experimental result and data into two basic data groups.

363 The concentrations of AuNPs and Au@Ag were proportional to the  
364 concentrations of the two corresponding illicit drugs. Therefore, the simultaneous  
365 quantification of two illicit drugs would be feasible through measuring the UV-vis  
366 spectra of these two noble metal nanoparticles. Through NMF analysis, we  
367 established a single quantitative analysis for two illicit drugs that worked even when it  
368 was difficult to quantify the targets in a complex sample because of the overlap of the  
369 two spectra. The target concentrations were quantified by analyzing the changes in the  
370 intensity of the signals of UV-vis spectra acquired by NMF. The interference of the  
371 spectral overlap between different UV-vis spectra-active nanoparticles could be  
372 solved automatically and easily through this data process system. The multivariate

373 evaluation scheme used in this assay could reduce the interference of spectral overlap  
374 on the scale of the whole UV-vis spectra rather than just a single peak as in their  
375 univariate counterparts. By using the relative intensities of the maximum peak  
376 intensity of Au@Ag NPs and AuNPs acquired from NMF, the results clearly  
377 demonstrated the real intensities of optical biosensor instead of the overlapping  
378 spectra (Figure S4). Figure S5 showed the quantitative result of the multiplexed  
379 determination of illicit drugs with two-colour colorimetry, which was almost in accord  
380 with Figure 3c and Figure 3d. Although the results verified the validity of the NMF  
381 system, the data before and after the NMF process echoed with each other and  
382 confirmed the feasibility of undisturbed linear analysis. As shown in Figure S5, the  
383 limit of detection (LOD) of METH was determined to be 0.5 nM, whereas the LOD of  
384 cocaine was 3.3 nM. The LOD of METH and cocaine were both lower than some  
385 previous reports (METH 50 nM (Shi et al., 2015) and cocaine 10 nM (Nie et al.,  
386 2013)), respectively, further illustrating the high sensitivity of our proposed approach.

387 In the presence of 7 illicit drugs and metabolites (1  $\mu$ M) other than METH,  
388 absorbance signals were nearly as low as that from the blank. Meanwhile, these  
389 signals were much lower than that with METH and cocaine, though the  
390 concentrations of all the other illicit drugs and metabolites were much higher than 50  
391 nM METH. What's more, compared with the blank the enhancement in absorbance  
392 intensity was not statistically significant among other illicit drugs, indicating that  
393 interference of these drugs to METH and cocaine determination was not specific  
394 (Figure 5a), which demonstrated that the affinity of illicit drug to certain  
395 corresponding aptamer was much better and higher than all other illicit drugs,  
396 rendering color array with wonderful specificity toward METH and cocaine. Taking  
397 into account the complex matrix of wastewater samples, if we want to use the



398 biosensor for evaluation the pattern of illicit drugs of abuse for WBE, it's worthwhile  
399 testing a large cohort of samples to for the calibration curves and improve reliability  
400 of our sensors

### 401 **3.5 Analysis of illicit drugs in wastewater with our biosensors**

402 To evaluate the ability of our colorimetric method for complex sample  
403 (wastewater) detection, we used our biosensors for the determination of METH (75  
404 nM nominal concentration) and cocaine (75 nM nominal concentration) spiked into  
405 the wastewater samples. As shown in Figure 5b, the result we detected for the colour  
406 signal intensity of wastewater with cocaine and METH was very much close to that  
407 from the buffer, while wastewater without cocaine and METH were all under the  
408 threshold value, indicating a negligible matrix effect on our sensing platform.  
409 Compared with the measured concentration and real concentration of illicit drugs, the  
410 average recovery of METH and COC in spiked effluent wastewater sample are 85.5%  
411 and 83.9%, respectively. The results showed great potential for our sensors for the  
412 multiplexed determination of illicit drugs in wastewater to evaluate of illicit drug  
413 consumption at the community level.

## 414 **4. Conclusions**

415 In summary, we have described non-aggregated noble metal nanoparticles (AuNPs  
416 and Au@Ag) based colorimetric method for the sensitive determination of illicit drugs  
417 using METH and cocaine determination as a case study. The biosensor consisted of  
418 RPs, CPs, and illicit drug-binding DNA aptamers, where the DNA aptamer could  
419 hybridize with both RP and CP, generating NPs-dsDNA-MBs sandwich structure.  
420 When an external magnetic field is used, the sandwich structure was removed from  
421 the solution, leading to the absorbance intensity decreasing. The absorbance intensity  
422 was correlated with the concentrations of illicit drugs, enabling the quantification of

423 the drugs. To solve the spectral overlap in this sensing platform, the information of  
424 supernatant was used for the quantification of multiplexed targets with an NMF  
425 analysis. Through an automatic NMF analysis, our colorimetric biosensors provided a  
426 simple and rapid quantification platform for two illicit drugs analysis at nM level in a  
427 single assay. These results showed that our proposed sensors have a huge potential on  
428 estimating the consumption of illicit drugs for WBE.

429 There is a growing requirement to monitor illicit drugs and other emerging  
430 contaminants in wastewater. Aptamers are synthetic single-stranded DNA which can  
431 specifically bind to a wide range of respective targets with a promising selectivity and  
432 sensitivity. This will enable our proposed biosensors to be used as a generic platform  
433 to detect a variety of contaminants by simply replacing certain corresponding  
434 aptamers, and easy to be improved from duplex assay to highly multiplexed  
435 determination for a range of substances. To obtain a reliably detection, it was  
436 suggested to test a large cohort of wastewater sample with a proper validation method.  
437 We believe that the rapid sensors will play an increasing role of monitoring of illicit  
438 drug of abuse and contribute as an alternative way for WBE.

### 439 **Acknowledgment**

440 We thank for NSFC grant (No. 41371442 and 41401566). ZY thanks UK NERC  
441 Fellowship grant (NE/R01334 9/1).

### 442 **References**

- 443 Asghary M, Raoof JB, Rahimnejad M, Ojani R. Microbial fuel cell-based self-powered biosensing  
444 platform for determination of ketamine as an anesthesia drug in clinical serum samples.  
445 *Journal of the Iranian Chemical Society* 2018; 15: 445-453.
- 446 Bade R, Tschärke BJ, White JM, Grant S, Mueller JF, O'Brien J, et al. LC-HRMS suspect screening to  
447 show spatial patterns of New Psychoactive Substances use in Australia. *Science of The Total*  
448 *Environment* 2019; 650: 2181-2187.
- 449 Berry MW, Browne M, Langville AN, Pauca VP, Plemmons RJ. Algorithms and applications for  
450 approximate nonnegative matrix factorization. *Computational Statistics and Data Analysis*  
451 2007; 52: 155-173.
- 452 Castrignanò E, Yang Z, Bade R, Baz-Lomba JA, Castiglioni S, Causanilles A, et al. Enantiomeric  
453 profiling of chiral illicit drugs in a pan-European study. *Water Research* 2018; 130: 151-160.

454 Cyranoski D. China expands surveillance of sewage to police illegal drug use. *Nature* 2018; 559: 310-  
455 311.

456 Du P, Li K, Li J, Xu Z, Fu X, Yang J, et al. Methamphetamine and ketamine use in major Chinese  
457 cities, a nationwide reconnaissance through sewage-based epidemiology. *Water Research*  
458 2015; 84: 76-84.

459 Du P, Zhou Z, Bai Y, Xu Z, Gao T, Fu X, et al. Estimating heroin abuse in major Chinese cities  
460 through wastewater-based epidemiology. *Science of The Total Environment* 2017; 605-606:  
461 158-165.

462 Du P, Zhou Z, Huang H, Han S, Xu Z, Bai Y, et al. Estimating population exposure to phthalate esters  
463 in major Chinese cities through wastewater-based epidemiology. *Science of The Total*  
464 *Environment* 2018; 643: 1602-1609.

465 EMCDDA. Assessing illicit drugs in wastewater: advances in wastewater-based drug epidemiology.  
466 2016.

467 Ettore Z, Chiara C, Sara C, Renzo B, Roberto F. Estimating community drug abuse by wastewater  
468 analysis. *Environ Health Perspect* 2008; 116: 1027-1032.

469 Foppe KS, Hammond-Weinberger DR, Subedi B. Estimation of the consumption of illicit drugs during  
470 special events in two communities in Western Kentucky, USA using sewage epidemiology.  
471 *Science of The Total Environment* 2018; 633: 249-256.

472 Galanie S, Thodey K, Trenchard IJ, Filsinger Interrante M, Smolke CD. Complete biosynthesis of  
473 opioids in yeast. *Science* 2015; 349: 1095-1100.

474 Gao T, Du P, Xu Z, Li X. Occurrence of new psychoactive substances in wastewater of major Chinese  
475 cities. *Science of The Total Environment* 2017; 575: 963-969.

476 Kumar V, Kumar P, Pournara A, Vellingiri K, Kim K-H. Nanomaterials for the sensing of narcotics:  
477 Challenges and opportunities. *TrAC Trends in Analytical Chemistry* 2018; 106: 84-115.

478 Li K, Qin W, Li F, Zhao X, Jiang B, Wang K, et al. Nanoplasmonic Imaging of Latent Fingerprints and  
479 Identification of Cocaine. *Angewandte Chemie* 2013; 125: 11756-11759.

480 Lodha A, Pandya A, Sutariya PG, Menon SK. A smart and rapid colorimetric method for the detection  
481 of codeine sulphate, using unmodified gold nanoprobe. *RSC Advances* 2014; 4: 50443-50448.

482 Mao K, Yang Z, Du P, Xu Z, Wang Z, Li X. G-quadruplex-hemin DNAzyme molecular beacon probe  
483 for the detection of methamphetamine. *RSC Advances* 2016; 6: 62754-62759.

484 Mao K, Zhou Z, Han S, Zhou X, Hu J, Li X, et al. A novel biosensor based on Au@Ag core-shell  
485 nanoparticles for sensitive detection of methylamphetamine with surface enhanced Raman  
486 scattering. *Talanta* 2018; 190: 263-268.

487 Merz F. United Nations Office on Drugs and Crime: World Drug Report 2017. 2017. SIRIUS -  
488 *Zeitschrift für Strategische Analysen*. 2, 2018, pp. 85.

489 Mokhtarzadeh A, Ezzati Nazhad Dolatabadi J, Abnous K, de la Guardia M, Ramezani M.  
490 Nanomaterial-based cocaine aptasensors. *Biosensors and Bioelectronics* 2015; 68: 95-106.

491 Neves MAD, Blaszykowski C, Bokhari S, Thompson M. Ultra-high frequency piezoelectric aptasensor  
492 for the label-free detection of cocaine. *Biosensors and Bioelectronics* 2015; 72: 383-392.

493 Nie J, Zhang D-W, Tie C, Zhou Y-L, Zhang X-X. A label-free DNA hairpin biosensor for colorimetric  
494 detection of target with suitable functional DNA partners. *Biosensors and Bioelectronics*  
495 2013; 49: 236-242.

496 Roncancio D, Yu H, Xu X, Wu S, Liu R, Debord J, et al. A Label-Free Aptamer-Fluorophore  
497 Assembly for Rapid and Specific Detection of Cocaine in Biofluids. *Analytical Chemistry*  
498 2014; 86: 11100-11106.

499 Shen A, Chen L, Xie W, Hu J, Zeng A, Richards R, et al. Triplex Au-Ag-C Core-Shell Nanoparticles  
500 as a Novel Raman Label. *Advanced Functional Materials* 20 2010: 969-975.

501 Shi Q, Shi Y, Pan Y, Yue Z, Zhang H, Yi C. Colorimetric and bare eye determination of urinary  
502 methylamphetamine based on the use of aptamers and the salt-induced aggregation of  
503 unmodified gold nanoparticles. *Microchimica Acta* 2015; 182: 505-511.

504 Song E, Han W, Li J, Jiang Y, Cheng D, Song Y, et al. Magnetic-Encoded Fluorescent Multifunctional  
505 Nanospheres for Simultaneous Multicomponent Analysis. *Analytical Chemistry* 2014; 86:  
506 9434-9442.

507 Stojanovic MN, De PP, Landry DW. Fluorescent Sensors Based on Aptamer Self-Assembly. *Journal of*  
508 *the American Chemical Society* 2000; 122: 11547-11548.

509 Tang D, Wang Q, Wang Z, Liu Q, Zhang B, He D, et al. Highly sensitive wearable sensor based on a  
510 flexible multi-layer graphene film antenna. *Science Bulletin* 2018; 63:574-579.

511 Thomas KV, Bijlsma L, Castiglioni S, Covaci A, Emke E, Grabic R, et al. Comparing illicit drug use in  
512 19 European cities through sewage analysis. *Science of The Total Environment* 2012; 432:  
513 432-439.

514 van Nuijs ALN, Castiglioni S, Tarcomnicu I, Postigo C, de Alda ML, Neels H, et al. Illicit drug  
515 consumption estimations derived from wastewater analysis: A critical review. *Science of the*  
516 *Total Environment* 2011; 409: 3564-3577.

517 Wen C-Y, Wu L-L, Zhang Z-L, Liu Y-L, Wei S-Z, Hu J, et al. Quick-Response Magnetic Nanospheres  
518 for Rapid, Efficient Capture and Sensitive Detection of Circulating Tumor Cells. *ACS Nano*  
519 2014; 8: 941-949.

520 Xie W, Herrmann C, Kömpe K, Haase M, Schlücker S. Synthesis of Bifunctional Au/Pt/Au Core/Shell  
521 Nanoraspberries for in Situ SERS Monitoring of Platinum-Catalyzed Reactions. *Journal of the*  
522 *American Chemical Society* 2011; 133: 19302-19305.

523 Xu Z, Du P, Li K, Gao T, Wang Z, Fu X, et al. Tracing methamphetamine and amphetamine sources in  
524 wastewater and receiving waters via concentration and enantiomeric profiling. *Science of The*  
525 *Total Environment* 2017; 601-602: 159-166.

526 Ya Y, Yifeng T, Xiaoshu W, Jinyin P, Yun D. A label-free immunosensor for ultrasensitive detection  
527 of ketamine based on quartz crystal microbalance. *Sensors* 2015; 15: 8540-9.

528 Yang Z, Castrignanò E, Estrela P, Frost CG, Kasprzyk-Hordern B. Community Sewage Sensors  
529 towards Evaluation of Drug Use Trends: Detection of Cocaine in Wastewater with DNA-  
530 Directed Immobilization Aptamer Sensors. *Scientific Reports* 2016; 6: 21024.

531 Zuccato E, Chiabrando C, Castiglioni S, Calamari D, Bagnati R, Schiarea S, et al. Cocaine in surface  
532 waters: a new evidence-based tool to monitor community drug abuse. *Environmental Health*  
533 2005; 4: 14.

534

### **Highlights**

- We developed a novel nanoparticles-based biosensor for the detection of illicit drugs.
- High selective and sensitive detection of two illicit drug (LOD of METH is 0.5 nM and cocaine is 3.3 nM) in a single assay.
- The biosensor enables a generic platform for the detection of illicit drugs in wastewater.

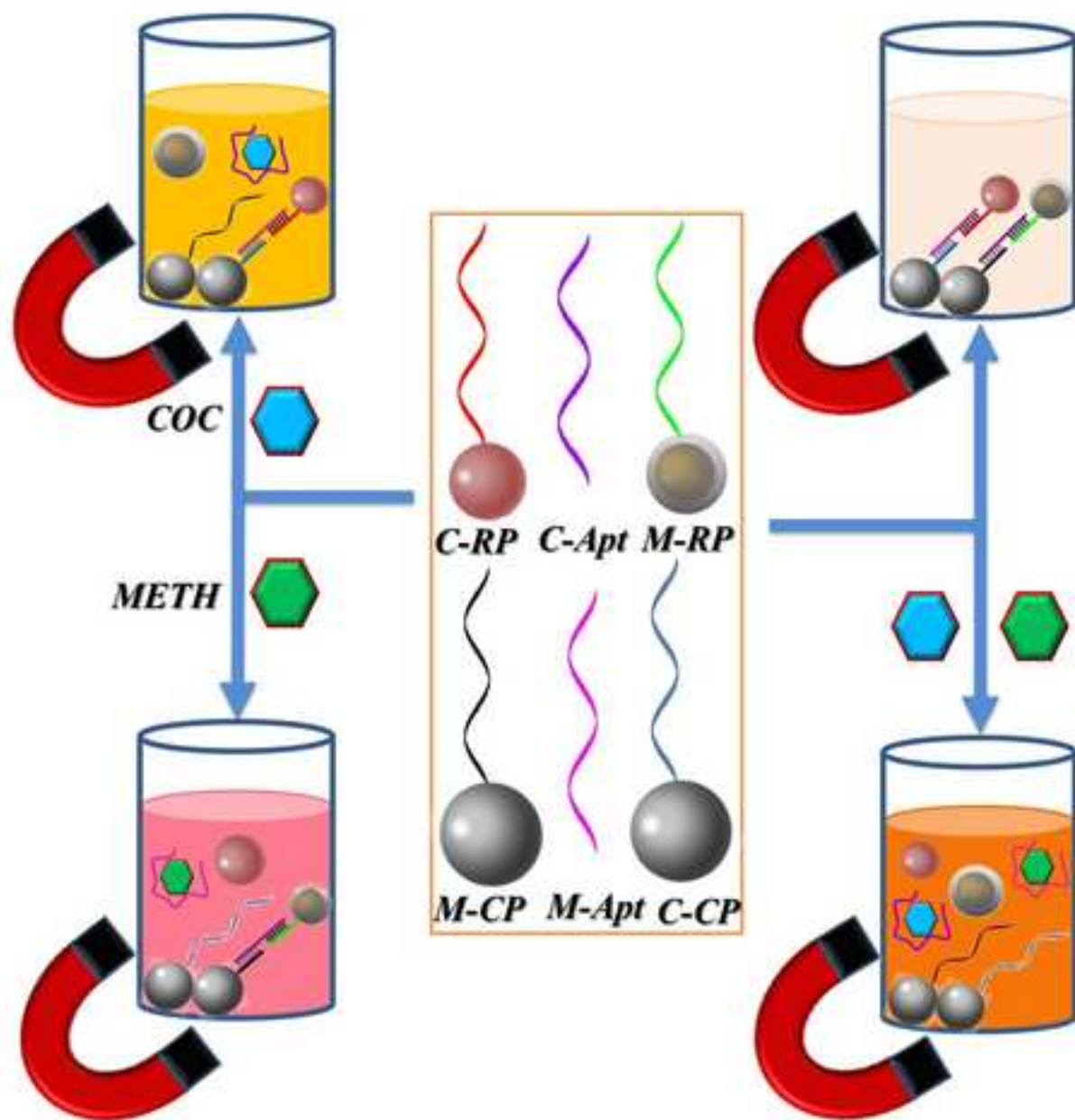
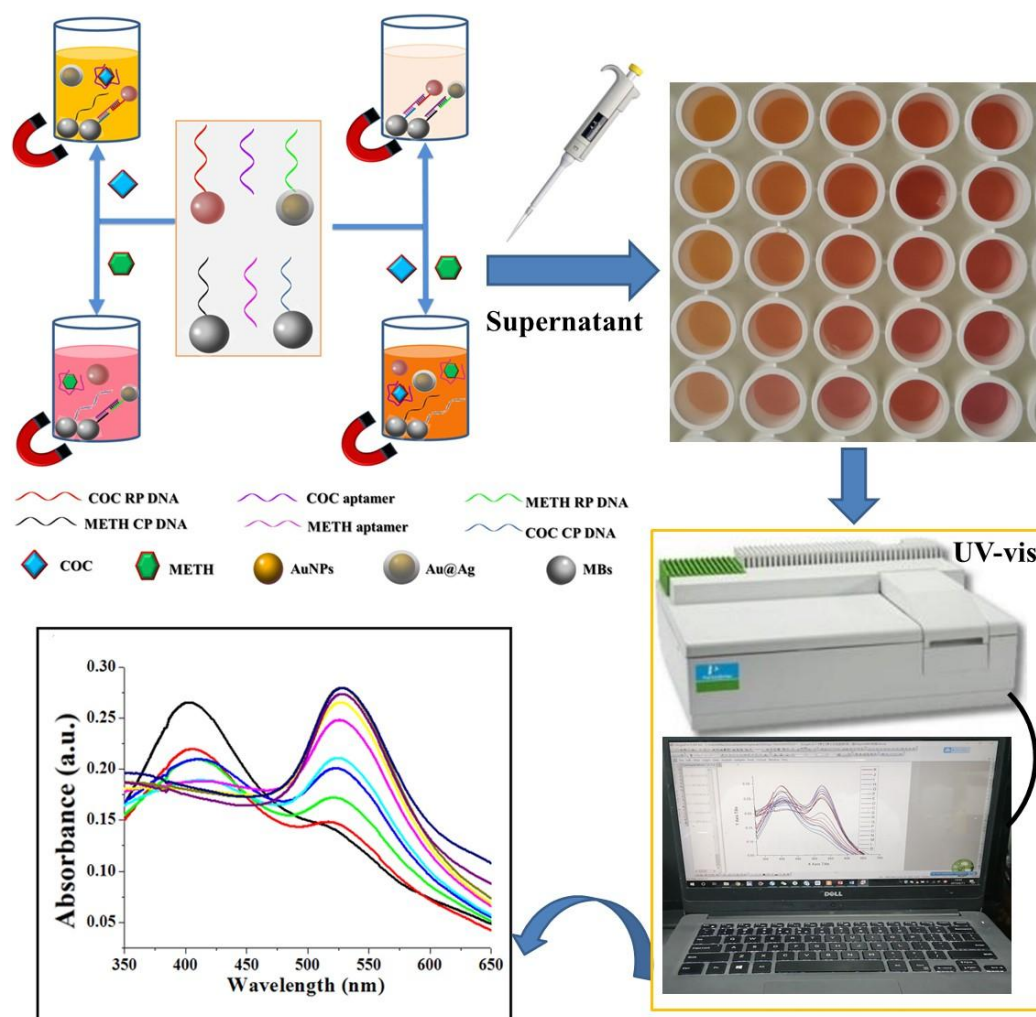


## Figure captions:



Scheme 1. Schematic illustration of colorimetric detection of METH and cocaine based on non-aggregated nanoparticles (C-RP: cocaine reporter probe, M-RP: methamphetamine reporter probe, M-CP, methamphetamine capture probe, and C-CP: cocaine capture probe).

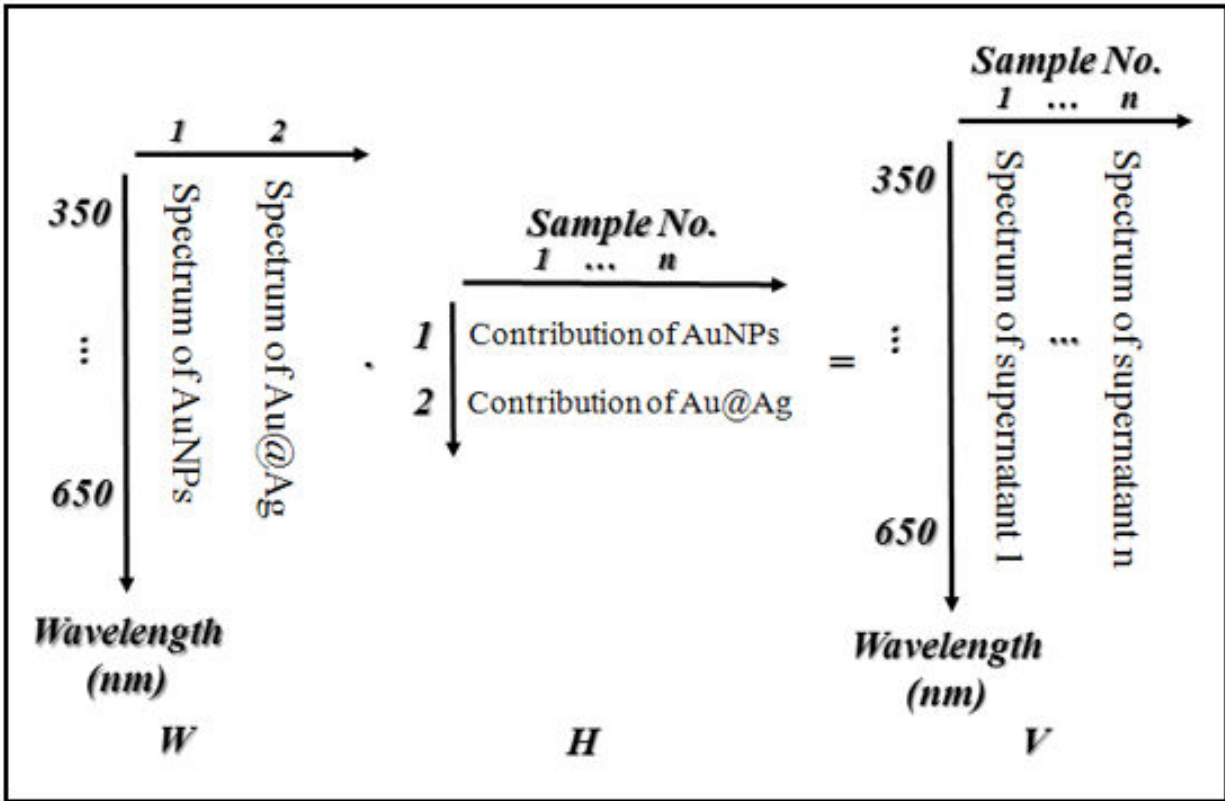


Figure 1. The principle of NMF analysis that processes the UV-vis spectra.



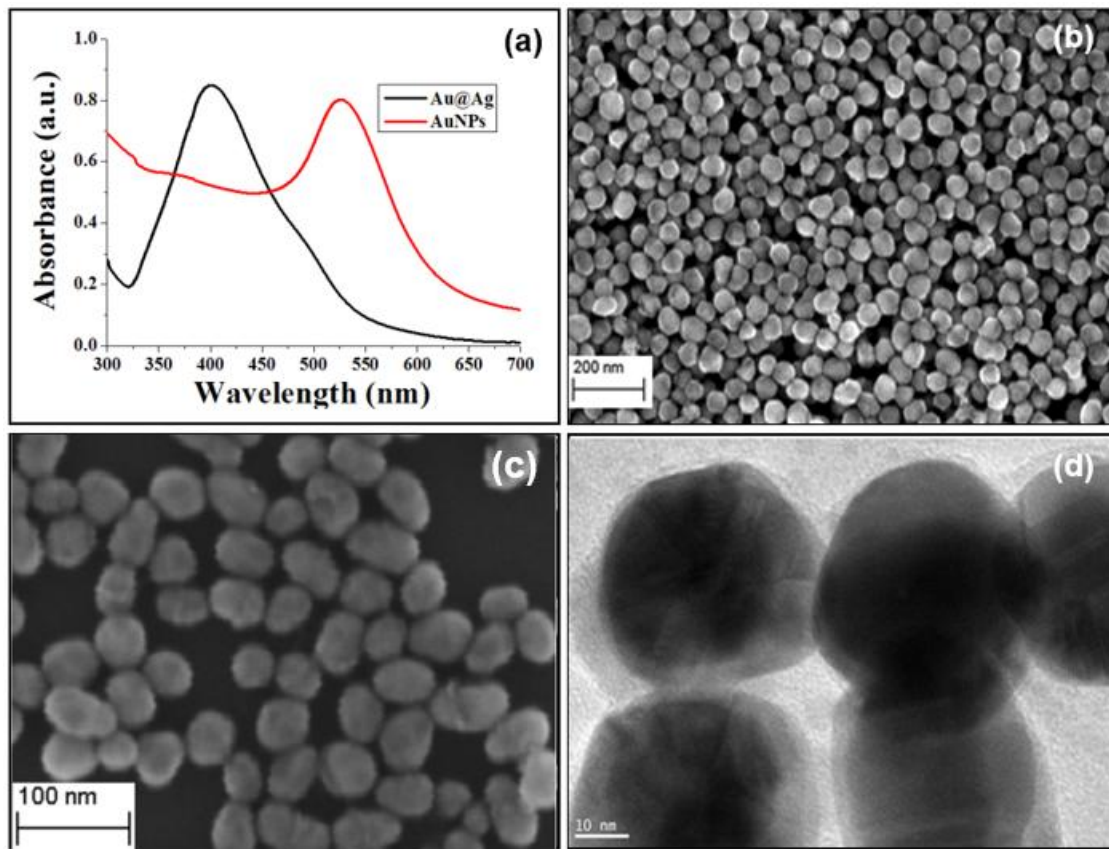


Figure 2. (a) UV-vis spectra of Au@Ag and AuNPs; (b) SEM image of AuNPs; (c) SEM image and (d) high resolution transmission emission microscope (HR-TEM) image of Au@Ag core-shell nanoparticles.

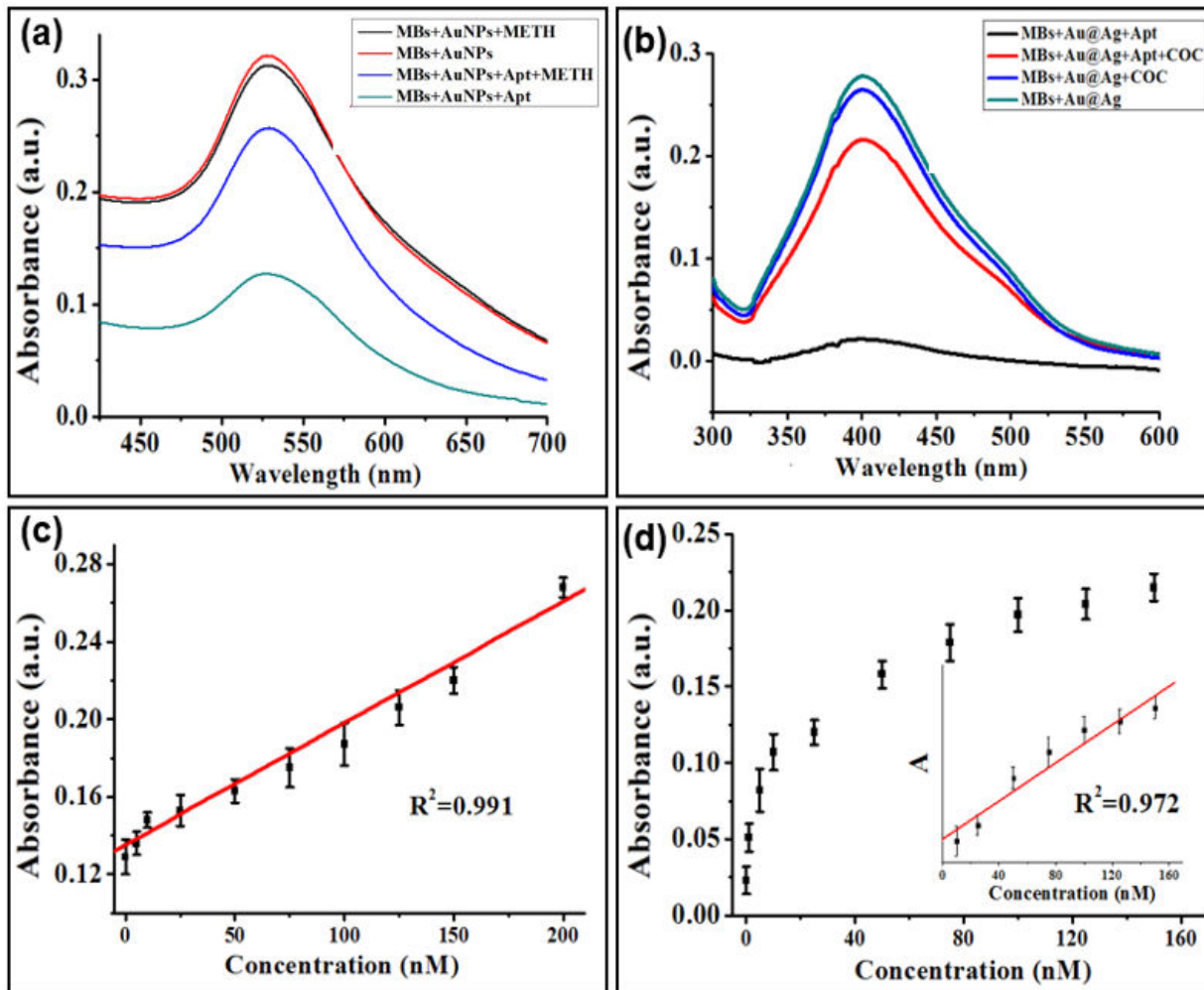


Figure 3. (a) UV-vis spectra of AuNPs in the presence of METH and control experiment; (b) UV-vis spectra of Au@Ag in the presence of COC and control experiment; (c) METH concentration-dependent change of SPR signal intensity ( $\lambda_{\max}=520$  nm) from 0 to 200.0 nM; (d) COC concentration-dependent change of SPR signal intensity ( $\lambda_{\max}=400$  nm) from 0 to 150.0 nM. The inset shows the linear range concentration from 10.0 to 150.0 nM, error bar representing at least three independent measurements.

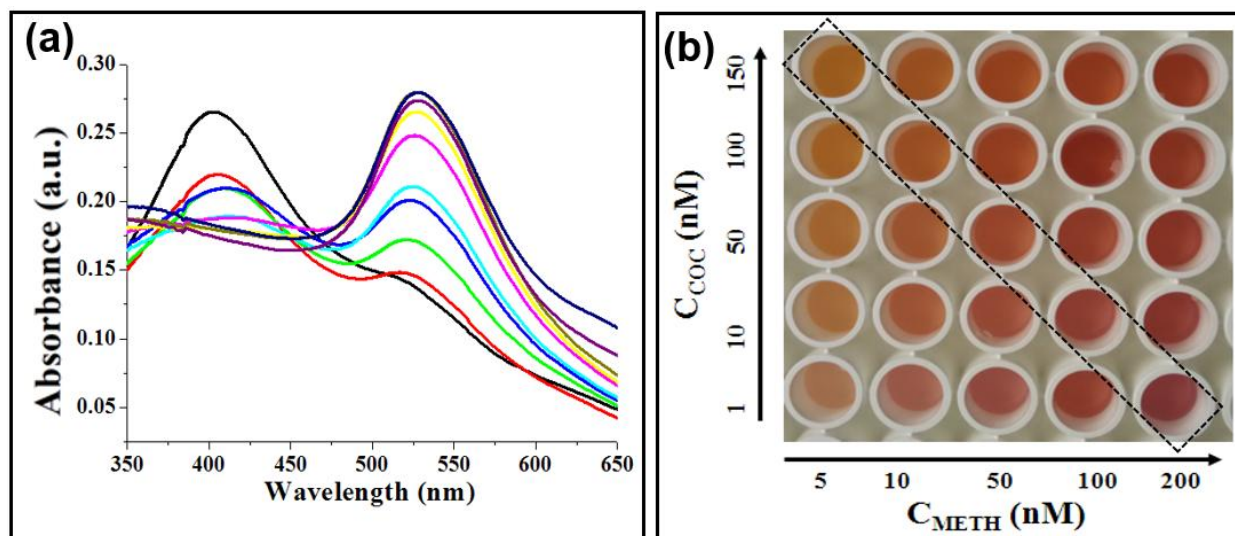


Figure 4. (a) UV-vis spectra of supernatant with the presence of different concentrations of METH and COC after incubation at 25 °C for 60 min (COC from bottom to top: 0, 1, 5, 10, 25, 50, 75, 100, 125, and 150 nM; METH from bottom to top: 0, 5, 10, 25, 50, 75, 100, 125, 150, and 200 nM.). (b) Photograph displaying the color change of the supernatant mixtures with different concentrations of targets (COC from bottom to top: 1, 10, 50, 100, and 150 nM; METH from left to right: 5, 10, 50, 100, and 200 nM).

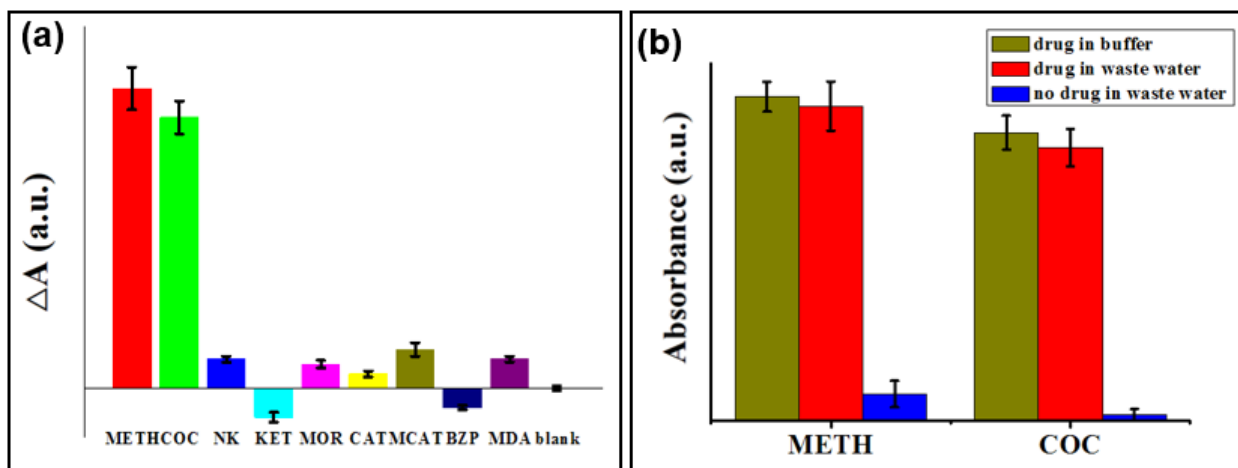


Figure 5. (a) Selectivity of the non-aggregation nanoparticles for METH and COC detection. The METH and COC concentration was 50 nM, while the concentrations of other illicit drugs were 1  $\mu$ M, METH, COC, NK, KET, MOR, CAT, MCAT, BZP, MDA, and blank. (b) Histogram for SPR intensities of METH and COC detection in wastewater. The signal ( $\Delta A$ ) represents the relative absorbance with respect to the blank and error bars represent three independent measurements.

# Rapid duplexed detection of illicit drugs in wastewater using gold nanoparticle conjugated aptamer sensors

Mao, Kang

2019-06-22

Attribution-NonCommercial-NoDerivatives 4.0 International

---

Mao K, Ma J, Li X, Yang Z. (2019) Rapid duplexed detection of illicit drugs in wastewater using gold nanoparticle conjugated aptamer sensors. *Science of the Total Environment*, Volume 688, October 2019, pp. 771-779

<https://doi.org/10.1016/j.scitotenv.2019.06.325>

*Downloaded from CERES Research Repository, Cranfield University*